Supporting Information

Explaining the Unusual Photoluminescence of Semiconductor Nanocrystals Doped Via Cation Exchange

Abigail R. Freyer[†], Peter C. Sercel[§], Zhentao Hou[†], Benjamin H. Savitzky[‡], Lena F. Kourkoutis[⊥,||], Alexander L. Efros[¶], Todd D. Krauss[,†,£]*

[†]Department of Chemistry and [£]The Institute of Optics, University of Rochester, Rochester, New York 14627-0216, United States

[§]T. J. Watson Laboratory of Applied Physics, California Institute of Technology, Pasadena, California 91125, United States

[‡]Department of Physics,[⊥]School of Applied and Engineering Physics, [||]Kavli Institute at Cornell for Nanoscale Science, Cornell University, Ithaca, New York 14853, United States

[¶]Naval Research Laboratory, Washington, D.C. 20375, United States

[*]Corresponding author. E-mail: krauss@chem.rochester.edu

[#]Current address: Department of Chemistry, Brown University, Providence, Rhode Island 02912, United States

Supporting Information

1. Materials and Methods

A. Chemicals and Substrates

Cadmium oxide (CdO, ≥99.99% trace metal basis), ethanol (solvent grade, 99.5%), hexanes (reagent grade, ≥98.5%), lithium nitrate ($LiNO_3$), 1-octadecene (ODE, technical grade, 90%), oleic acid (technical grade, 90%), selenium pellets (Se, <5 nm, ≥99.99% trace metal basis), silver nitrate ($AgNO_3$, 99.9999% trace metal basis), silver perchlorate ($AgClO_4$, anhydrous, 97%), toluene (solvent grade, ≥99.5%), trioctylphosphine (TOP, technical grade, 90%), and nitric acid (HNO_3, TraceSELECT, ≥69.0%) were purchased from Sigma-Aldrich. Calcium nitrate ($Ca(NO_3)_2$) was purchased from VWR. Polyvinyl butyral (PVB, Butvar B-98) was purchased from Fisher Scientific. Cadmium (Cd, 10 ppm in HNO_3), indium (In, 10 ppm in HNO_3), selenium (Se, 10 ppm in HNO_3), and silver (Ag, 10 ppm in HNO_3) ICPMS standards were purchased from Inorganic Ventures. All chemicals were used as delivered without further purification. Highly oriented pyrolytic graphite (HOPG, grade SPI-2) was purchased from SPI Supplies.

B. Synthesis of CdSe Nanocrystals

CdSe NCs were made with known synthesis procedures.[1,2] A 0.2 M cadmium oleate precursor was made adding CdO (3.18 g, 24.8 mmol), ODE (90 mL, 280 mmol), and oleic acid (34.5 mL, 108 mmol) together in a 250-mL round bottom flask. With condenser, stirring, and under N_2 flow, the reaction flask was heated to 220°C for about one hour until everything was dissolved. The flask was cooled until the solution became a white, waxy solid. A 1 M trioctylphosphine selenide (TOPSe) precursor was made by dissolving Se pellets (0.7896 g, 10 mmol) in TOP (10 mL, 22 mmol) in a N_2-filled glovebox. The reaction mixture was heated to 60°C with stirring until dissolved.

For the NC synthesis, the cadmium oleate precursor was melted at approximately 60°C under N_2 with stirring. In a 100-mL flask, 0.2 M cadmium oleate (30 mL, 6 mmol) and ODE (20 mL, 62 mmol) were heated to 270°C under N_2 with stirring. Once at 270°C, 1 M TOPSe (2 mL, 2 mmol) was injected rapidly. Immediately following TOPSe injection, the reaction temperature was set to 220°C and the NCs were allowed to grow for 6 minutes. After 6 minutes, the NC solution was cooled to room temperature. This synthesis consistently produced CdSe NCs with an average diameter of 2.9-3.2 nm.

To ensure the removal of excess ligands and to redisperse in an alternate solvent, a rigorous washing procedure was followed. The NCs were washed by precipitation in ethanol with centrifugation. The NCs were redispersed in hexanes and the precipitation step was repeated two additional times with final redispersion of the NCs in toluene.

C. Doping of CdSe Nanocrystals with Cations

The CdSe NCs were doped with Ag^+ ions following the cation exchange doping procedure established by Sahu *et al.*[3] Samples with a range of Ag amounts added were prepared in order to study the effects of dopant concentration. In order to do this, the concentration of the washed NC solution was determined from the absorbance following the method described by Yu *et al*.[4] From this concentration and the assumed composition of the CdSe unit cell, the Cd concentration was calculated. Ag was added in different Ag:Cd ratios based on this calculated Cd concentration to

create the range of dopant concentrations. $AgNO_3$ was used as the Ag precursor; 0.1 M and 0.02 M $AgNO_3$ solutions in ethanol were prepared and used for the doping. The different $AgNO_3$ concentrations were used in order to keep the added volume of the ethanolic solution approximately constant and to maintain a similar end volume.

For the doping procedure, an oil bath was heated to 60°C on a stir plate. Vials with the NC toluene solution were placed in the oil bath with stirring. After 5 minutes, time to let the temperature of the NC solution to equilibrate, TOP was added, in the volume of 5% of the initial NC solution volume. Precisely 30 seconds later, the $AgNO_3$ in ethanol was added (volume and concentration depending on the desired Ag:Cd ratio). One minute later, ethanol was added (2.5x the original NC solution volume) in order to quench the cation exchange doping reaction. Three minutes later, the solution was centrifuged to allow for NC precipitation. The resulting NCs were dispersed in toluene (volume equal to the original NC solution volume). Typically, this doping procedure was carried out on a NC solution volume of 3-4 mL.

For the introduction of the additional ions studied, an identical doping process to that with Ag was followed. The sole difference was the introduction of the other salt solutions ($LiNO_3$, $Ca(NO_3)_2$, and $AgClO_4$ all in ethanol) instead of the $AgNO_3$ in ethanol. These salts were chosen in order to study the effects of introducing a different +1 cation, doping with a +2 cation, and doping in the presence of a different anion, respectively. The Li^+ and Ca^{2+} cations were also chosen because of their solubility in ethanol, the solvent used for the $AgNO_3$ doping, and because of their fairly comparable ionic radii to that of Ag^+.[5] Similar concentrations of these salt solutions were used. All samples were kept in vials wrapped in parafilm and stored in the dark.

D. Sample Characterization

Ultraviolet-visible (UV-Vis) absorption spectrophotometry, fluorescence spectroscopy, time correlated single photon counting (TCSPC), high angle annular dark field-transmission electron microscopy (HAADF-TEM), inductively coupled plasma-mass spectrometry (ICP-MS), X-ray diffraction (XRD), and atomic and electrostatic force microscopies (AFM and EFM) were used to characterize the size, composition, and optical and electrostatic properties of the doped NCs.

Optical characterization was performed on NCs dispersed and diluted in toluene in a 1 cm path length quartz cuvette. Absorption spectra were obtained using a PerkinElmer Lambda 950 UV/VIS spectrophotometer. Photoluminescence (PL) spectra were collected using a home-built fluorometer system with a 450 W xenon arc lamp source coupled to an excitation SpectraPro 150 monochromator. A photomultiplier tube (PMT) was used for emission detection with an emission SpectraPro 300i monochromator every 1 nm with an integration time of 100 ms. The excitation wavelength was 480 nm for all of the PL spectra obtained.

TCSPC was used to measure the PL lifetimes. For this measurement, approximately 10 μL of a diluted sample solution was dropped onto a glass coverslip. The sample was photoexcited with a 488 nm diode laser with a circularly polarized beam and repetition rate of 2.5 MHz. A neutral density filter wheel was used to maintain a photon flux low enough to provide less than 0.2 photoexcited excitons per NC per pulse. A Si avalanche photodiode with a timing resolution of less than 50 ps was used to detect the NC PL. The instrument response function was measured from residual scattering of the laser beam. PL decay curves were analyzed using FluoFit software and fitted with a biexponential decay of the form $I(t) = A_1 e\left(-\frac{t}{\tau_1}\right) + A_2 e(-\frac{t}{\tau_2})$. The average lifetime τ was calculated using $\tau = \frac{A_1\tau_1^2 + A_2\tau_2^2}{A_1\tau_1 + A_2\tau_2}$ and the amplitude weighted lifetime was calculated as $\tau_{aw} = A_1\tau_1 + A_2\tau_2$ where $A_I\tau_I$ is the

integrated intensity of light that decay for the time τ_1. The radiative and non-radiative rates were calculated as $k_{rad} = \frac{QY}{100 \times \tau}$ and $k_{nr} = \frac{1}{\tau} - k_{rad}$, respectively, where QY is the quantum yield determined experimentally.

In order to clean up the sample for HAADF-TEM imaging, the NC solutions were washed by precipitation with ethanol and redispersion in hexanes an additional three times. The final NC solutions used for spotting were in hexanes. Samples were drop cast onto TEM grids with an ultrathin, nominally 2-3 nm amorphous carbon support layer. Imaging was performed on an aberration-correct FEI Titan operating in HAADF-STEM mode at an accelerating voltage of 60 keV and with a 21 mrad convergence semi-angle. To minimize sample contamination, data was acquired under in-situ liquid nitrogen cooling. To account for stage instabilities introduced by cryogenic cooling and obtain high SNR atomic resolution images, fast acquisition image stacks were obtained, aligned, and averaged.[6]

ICP-MS analysis was performed with an Agilent 7900 ICP-MS system. For calibration, the sample data was compared to intensities of four separate single-element standards, Ag, Cd, Se, and In, purchased from Inorganic Ventures. ^{115}In was used as an internal standard. For ICP-MS, the samples were prepared first by precipitating out the NCs by adding ethanol and centrifuging (after multiple successive precipitation/redispersion washing steps). The NCs were allowed to dry and then the NC pellet was digested in spectroscopy-grade concentrated nitric acid. The NC nitric acid solution was diluted, resulting in a ~2% nitric acid solution with <10 ppm concentrations of Cd, Se, and Ag. The Ag:Cd ratio was determined using the ratio of the respective concentrations for each solution. The Ag/NC concentration was then estimated by comparing the atomic density of Cd within a CdSe crystal of known size, as determined through TEM and absorption spectra, with the total amount of Cd present, as determined through ICP-MS. Note that this technique only provides an ensemble average Ag/NC concentration and not information about a specific NC nor the distribution of Ag among NCs.

For XRD measurements, the NC toluene solution was dropped onto a low background quartz holder and the toluene was allowed to evaporate. This process was repeated a number of times to get a film of NCs on the holder. The instrument used was a PANalytical Multi Purpose Diffractometer (MPD) consisting of a PW1830 controller and PW3020 goniometer. Cu radiation was used at 40 kV and 30 mA.

E. Electrostatic Force Microscopy Measurements

EFM sample preparation: A thin layer of PVB was coated onto the surface of the HOPG substrate by spin coating 30 μL of a 0.05% PVB in toluene solution for 60 seconds at 3000-4000 rpm. A dilute QD solution (in toluene) was then spin coated, again 30 μL for 60 seconds at 3000-4000 rpm.

AFM and EFM images were obtained at room temperature with an Asylum MFP-3D-BIO AFM inside an acoustic hood purged with N_2 to <17% relative humidity using the Asylum Research Version 12 software. Olympus-made AC240TM-R3 titanium-platinum-coated silicon cantilevers with spring constants of ~1.2-1.8 N/m from Asylum Research were used at their resonant frequencies of 62-71 kHz. In order to obtain topographical AFM images and electrostatic EFM images simultaneously, the microscope made two passes for each scan. Two lock-in amplifiers were used to simultaneously measure the $\Delta\nu(\omega)$ and $\Delta\nu(2\omega)$ signals. Typical parameters were: V_{ac} = 3 V peak-to-peak, ω = 400 Hz, lock-in time constant = 3 ms, scan rate = 0.75 Hz per line, and lift-height z = 5-8 nm. The acquisition time for a complete image was approximately 11 minutes. Images were

recorded such that $V_{dc} = -\phi$ (typically, $|V_{dc}| < 0.7$ V). Curve fitting and image analysis were performed with Igor Pro 6.3.7.2 and calculations were performed with Wolfram *Mathematica* 10.

2. Electrostatic Force Microscopy Explanation

A. Equations and theory

EFM measures electrostatic forces between a conductive cantilever and conductive substrate in a modified AFM experiment. EFM consists of two passes of a line scan, a first pass equal to a normal AFM pass and a second pass with the tip lifted off the surface and scanned with an applied voltage.[7,8] The attractive force between the cantilever and the substrate with the applied voltage is proportional to the square of the voltage difference between the cantilever and the substrate.

$$F = \frac{1\partial C}{2\partial z}V^2 \qquad \text{(S1)}$$

The application of a sinusoidal voltage, $V=V_{dc}+V_{ac}sin(wt)$, results in an electrostatic attraction with components at zero frequency, at the frequency of the applied voltage, ω, and at twice that frequency, 2ω. With lock-in amplification, the components of the force on the tip at ω and 2ω, the capacitive and Coulombic forces, respectively, can be determined:[9,10]

$$F(\omega) = \left(\frac{\partial C}{\partial z}(V_{dc} + \phi) + \frac{QC}{4\pi\epsilon_0(z+R)^2} + \frac{Q_1 C}{4\pi\epsilon_0\left(z + R + \frac{2h}{\epsilon_1}\right)^2} + \frac{\partial C Q_2}{\partial z\, C}\right)V_{ac} \qquad \text{(S2)}$$

$$F(2\omega) = \frac{\partial C {V_{ac}}^2}{\partial z\ \ 4}. \qquad \text{(S3)}$$

The EFM tip is modeled as a cone with a sphere end with radius R. C is the capacitance between the EFM tip and the substrate, z is the separation between the insulator surface and the bottom of the EFM tip, and ϕ is the contact potential difference between the tip and the substrate. The samples consist of a metallic highly oriented pyrolitic graphite substrate with the nanocrystals atop a thin insulator layer with thickness h and dielectric constant ε_1. Q_1 and Q_2 are induced charges on the metallic substrate and the EFM tip, and assuming a parallel plate geometry between the tip and substrate,

$$Q_1 = -Q\frac{z}{\left(\frac{h}{\epsilon} + z\right)} \qquad \text{(S4)}$$

$$Q_2 = -Q\left(1 - \frac{z}{\left(\frac{h}{\epsilon} + z\right)}\right). \qquad \text{(S5)}$$

An oscillating AFM tip is effectively a simple harmonic oscillator in a force field, and as such, its resonant frequency is[8,10]

$$\nu = \nu_0\sqrt{1 - \frac{1\partial F}{\kappa \partial z}} \qquad \text{(S6)}$$

where κ is the cantilever spring constant and ν_0 is the natural resonance frequency. With small force gradients, such that $\Delta\nu = \nu - \nu_0 \ll \nu$, ν can be approximated by the first two terms of the Taylor expansion in dF/dz and the change in resonant frequency is

$$\Delta\nu = \frac{-\nu\partial F}{2\kappa\ \partial z}. \qquad \text{(S7)}$$

With no sample present, EFM can be used to measure the capacitance of the tip-substrate system, which, with its derivatives, is needed for an absolute determination of Q.[8,10] Taking the derivative of equation (S2) with no charges present and inserting it into equation (S7) gives

$$\frac{\partial^2 C}{\partial z^2} = \frac{-2\kappa \quad \Delta\nu(\omega)}{(V_{dc} + \phi)V_{ac} \quad \nu} \qquad \text{(S8).}$$

From this equation, the capacitance between the EFM tip and the substrate can be obtained by holding V_{ac} and V_{dc} fixed.

The capacitance of the tip-substrate system can be measured and subsequently used to determine the surface charge, Q, from the measured force gradient on the tip at ω.[11] Dielectric properties can be determined by fitting the measured force on the cantilever at 2ω.[10] EFM allows for the facile determination of the dielectric constants and surface charges of individual NCs. The response of the oscillating cantilever at twice the frequency of the applied voltage, $\Delta\nu(2\omega)$, yields the capacitive force information from which the dielectric constant can be determined. An increase in magnitude in the presence of a NC is expected due to the larger dielectric constant of CdSe compared to the surroundings. Similarly, the response of the cantilever at the frequency of the applied voltage, $\Delta\nu(\omega)$, measures local electrostatic potential variations and allows for determination of the charge magnitude. For a charge image, with V_{dc} set to zero out the contact potential difference, three types of behavior are possible: an increase or decrease in the measured Coulombic force corresponding to a positive or negative charge, respectively, or a static force corresponding to a neutral NC.

B. Cantilever-substrate capacitance

In order to use EFM and the given equations to calculate the charges and dielectric constants of the NCs studied, the capacitance needs to be determined. Experimentally holding V_{ac} and V_{dc} fixed and putting the measured $\Delta\nu(\omega)$ as a function of z into equation (S8), the second derivative of the capacitance between the EFM tip and the substrate was obtained. The experimental data was fit to a sphere-cone capacitor model as described by Cherniavskaya *et al.*[8], given in equations (S9) through (S11) and shown in Figure S1. In the given equations, ρ is the tip radius and θ is the cone angle. The terms α and β describe contributions of the tip radius and cone angle, respectively: $\alpha = \ln\left(1 + \sqrt{\frac{z^2}{\rho^2} + \frac{2z}{\rho}} + \frac{z}{\rho}\right)$ and $\beta = \ln\left(\frac{1+\cos\theta}{1-\cos\theta}\right)$. The total sphere-cone model fit was integrated in order to determine the capacitance of the EFM capacitor, which was in turn used to calculate both the charge and dielectric constant of the various NCs studied using the equations given above.

$$C_{total} = C_{sphere} + C_{cone}. \qquad \text{(S9)}$$

$$C_{sphere} = 4\pi\epsilon_0\rho + 4\pi\epsilon_0\rho\sum_{n=2}^{\infty}\frac{\sinh\alpha}{\sinh n\alpha} \quad \text{(S10)}$$

$$\beta = \ln\left(\frac{1+\cos\theta}{1-\cos\theta}\right) \quad \text{(S11)}$$

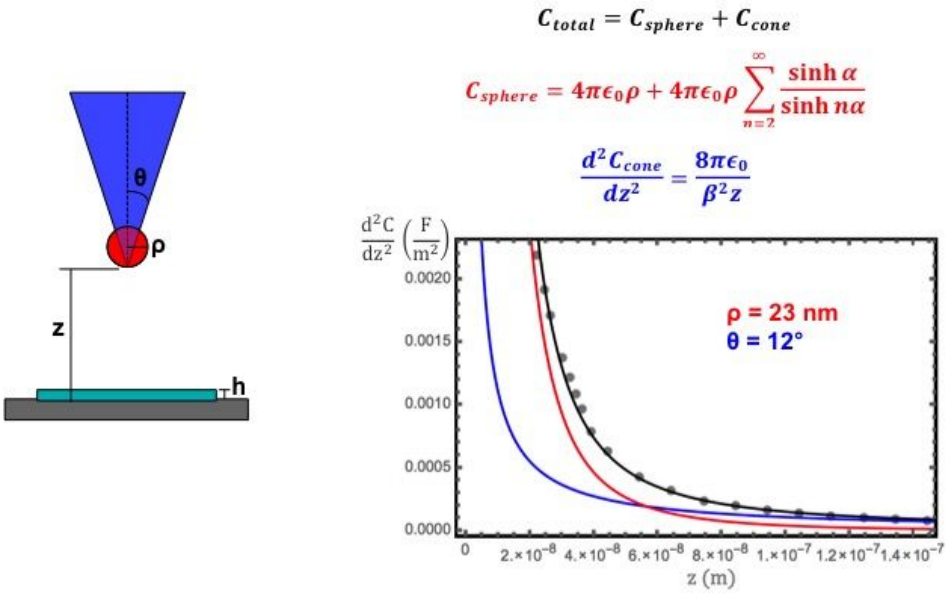

Figure S1. (left) Diagram of the cone-sphere tip geometry that contributes to the total capacitance of the tip-substrate system with tip parameters labeled. (right) Cone-sphere model fit of the tip-surface interactions to experimental d^2C/dz^2 vs. z data. The black, red, and blue solid lines are the sphere-cone fit and sphere and cone contributions, respectively, as determined with the equations given in corresponding colors. The grey circles describe the experimental data. Tip parameters determined for this set of data are given on the plot.

C. Photoexcitation calibration experiment

It has been shown that upon photoexcitation, CdSe NCs see an increase in their charge by 1e as a photoexcited electron tunnels through the polymer insulator later into the metallic HOPG substrate.[7] Then, upon termination of the excitation, an electron tunnels back into the NC. This process is described by the schematic given in Figure S2c. A similar photoexcitation experiment was performed here to calibrate the system and check the accuracy of the calculations performed. A set of NCs shown in the height image in Figure S2a where photoexcited with a Coherent 530 nm CW diode laser at a grazing angle. EFM images were continuously obtained for these NCs over time before, during, and after the excitation. Representative $\Delta\nu(\omega)$ charge images across this time are given in Figure S2b. As seen in these charge images, the starting NCs are bright as they are negatively charged. Upon excitation, the NCs start to lose brightness as they lose an electron and become more positive. Finally, after the termination of the excitation, the NCs start to return to their original charge signals as an electron tunnels back into the NCs.

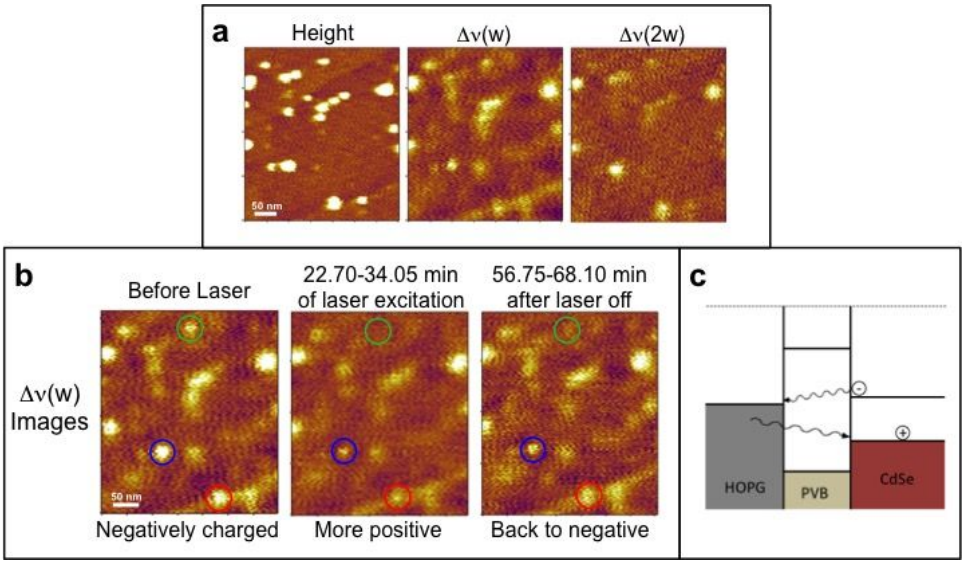

Figure S2. (a) Set of EFM images of an undoped NC sample with the height, charge, and dielectric images given left to right. (b) Charge images given for the same set of NCs taken at various time points. The left image shows the NCs before photoexcitation, the middle image was taken during photoexcitation, and the right image was taken about an hour after the photoexcitation ended. The green, blue, and red circles highlight three sample NCs across the images. (c) A schematic of the energy levels of the substrate-sample system diagraming the course of electrons upon photoexcitation of the NCs.

The $\Delta\nu(\omega)$ value was collected for 17 individual NCs at 11 different time points each, giving 187 total data points, as given in Figure S3a. "Time traces" for the individual NCs were plotted with each data point connected by a solid line for a particular NC. The representative time used for each data point was taken as the starting time of each image. Vertical dotted lines in Figure S3a represent the times at which the laser photoexcitation started and ended. The average charge signal of the 17 NCs at each time point is given by the solid black line. As seen in the negative slope of the black line between the starting and end points of photoexcitation, on average, the NCs do see a decrease in their $\Delta\nu(\omega)$ signal (an increase in charge). The 187 obtained $\Delta\nu(\omega)$ values were culminated into a histogram as given in Figure S3b. Gaussian fits are overlaid on the histogram to show distributions of NCs giving certain $\Delta\nu(\omega)$ signals. From both the "time traces" and the histogram, discrete $\Delta\nu(\omega)$ signal jumps are seen, with the discrete difference corresponding to a 1e charge. This distinction was also confirmed by calculating the charge from the $\Delta\nu(\omega)$ signal value using the given equations, with 0.35 V corresponding to approximately 1e from the calculations for this specific experiment.

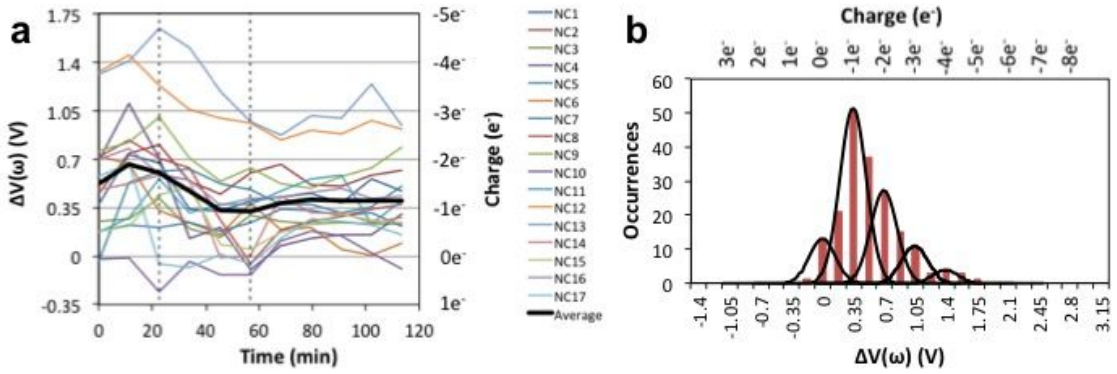

Figure S3. Photoexcitation calibration experiment. (a) "Time traces" for 17 individual NCs with data collected from 11 images per NC connected by solid lines. The representative time for each data point was taken as the starting time of each image. Vertical dotted lines represent the times at which the laser photoexcitation was started and ended, respectively. (b) The charge signal data for every NC at each time point presented in a histogram. The plots list both the raw $\Delta v(\omega)$ data and the charges calculated from the raw data.

3. Additional Data

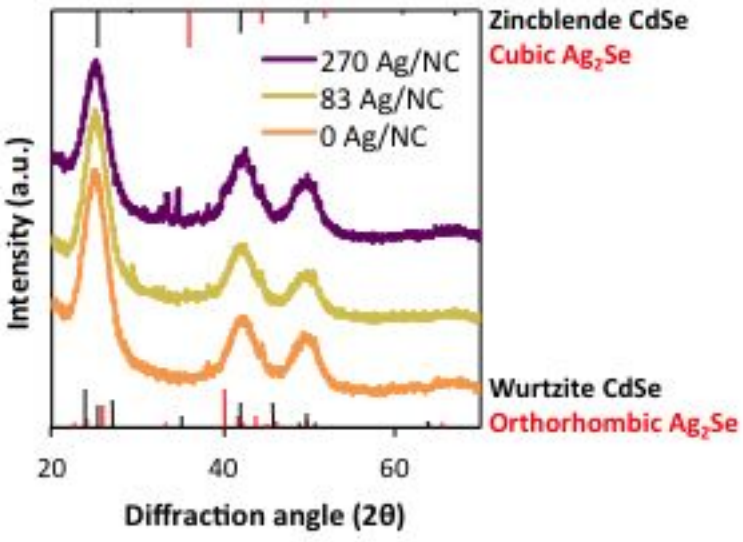

Figure S4. XRD patterns for samples with varying amounts of Ag/NC with the reference patterns of zincblende and wurtzite CdSe (in black) and cubic and orthorhomic Ag_2Se (in red) showing the presence of zincblende CdSe NCs in the samples, regardless of Ag concentration.

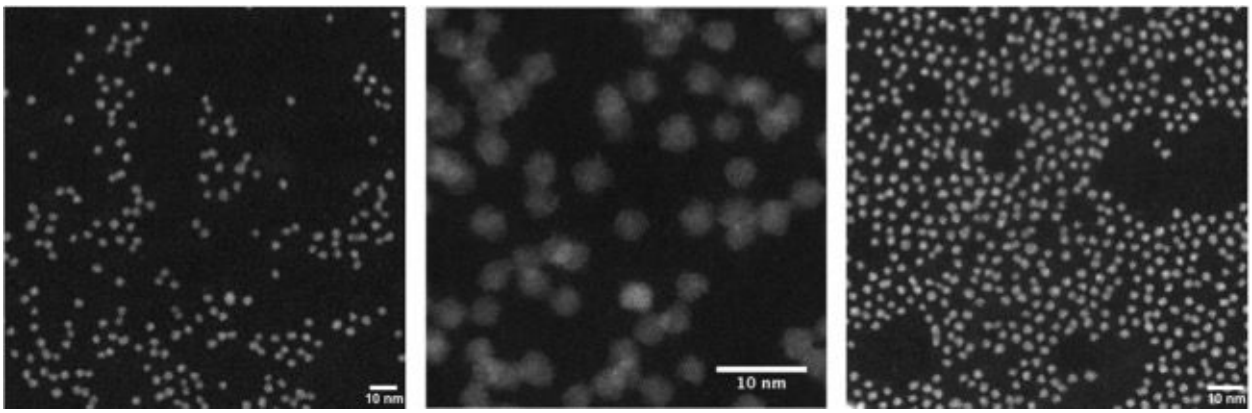

Figure S5. Lower magnification ADF-STEM images for samples of (a) 0 Ag/NC, (b) 83 Ag/NC, (c) 270 Ag/NC. Scale bars represent 10 nm in each image.

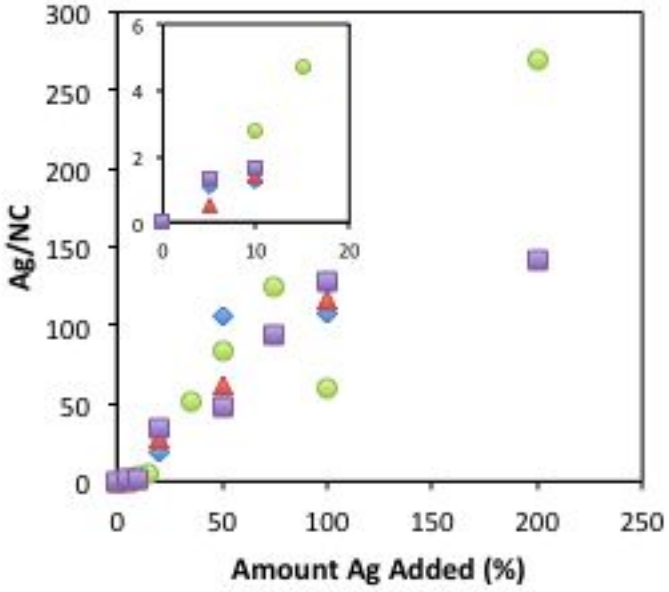

Figure S6. The number of incorporated Ag atoms per NC, determined by ICP-MS vs. the amount of Ag added to the exchange reaction, reported as a Ag/Cd molar percentage. As expected, as the amount of Ag added increases, the number of Ag/NC also increases.

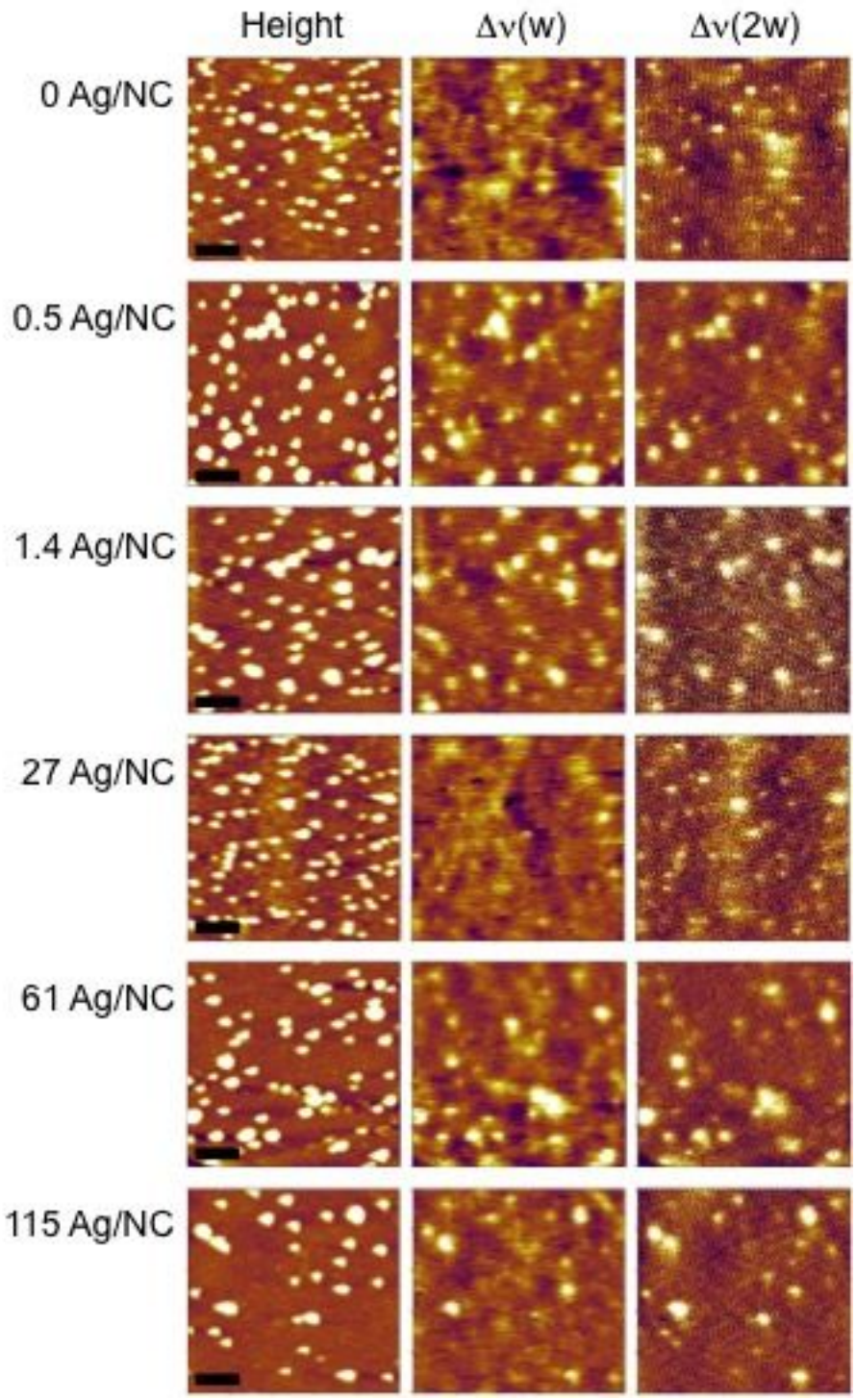

Figure S7. EFM images for a series of Ag^{+} doped CdSe NCs with the height, charge, and dielectric images given left to right for each sample. Scale bars represent 100 nm. Additional optical and EFM data for this particular doping series are given in Figure S9.

Given below are optical and EFM data for additional doping sets, including sets of $AgNO_3$ doping of CdSe NCs and of $AgClO_4$, $LiNO_3$, and $Ca(NO_3)_2$ doping of CdSe NCs.

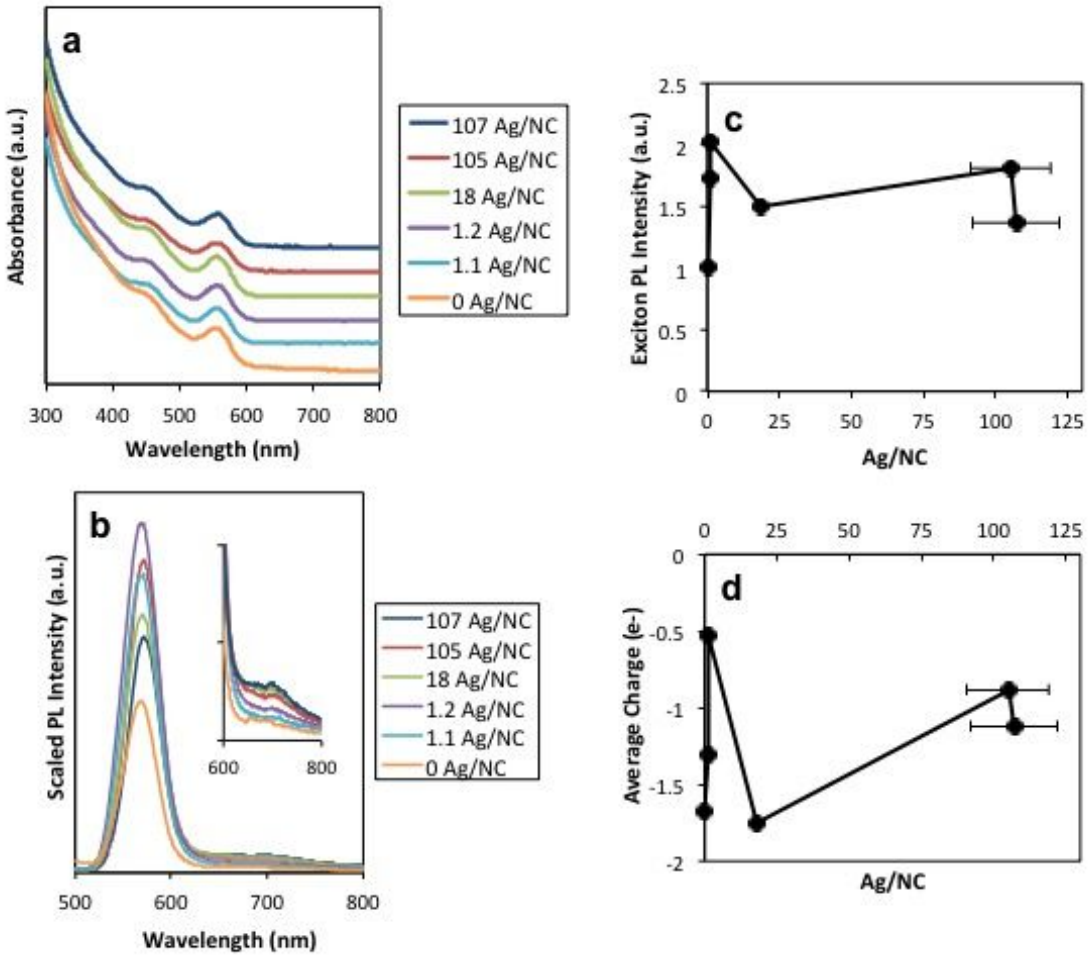

Figure S8. (a) Absorbance and (b) PL spectra for a set of Ag-CdSe NC doping. The inset in (b) magnifies the weak fluorescence feature near 700 nm. (c) The maximum exciton PL intensities and (d) the average charges vs. Ag/NC for this trial of Ag-CdSe.

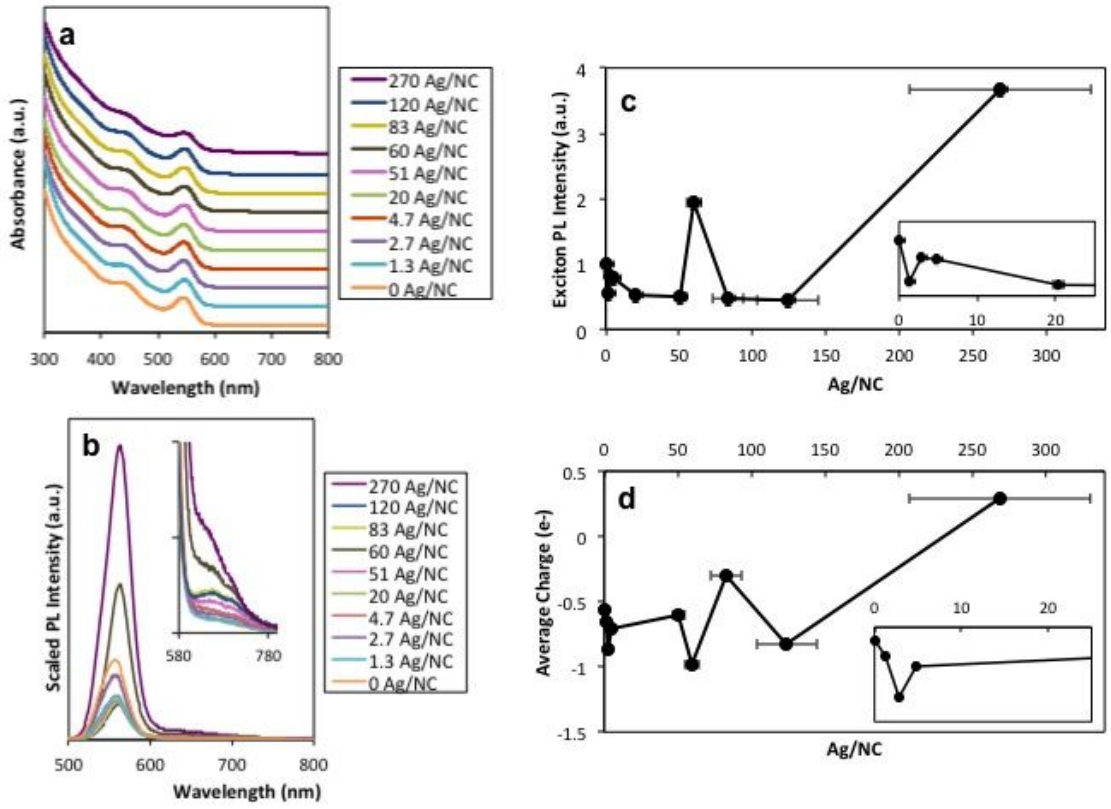

Figure S9. (a) Absorbance and (b) PL spectra for a set of Ag-CdSe NC doping. The inset in (b) magnifies the weak fluorescence feature near 700 nm. (c) The maximum exciton PL intensities and (d) the average charges vs. Ag/NC for this trial of Ag-CdSe.

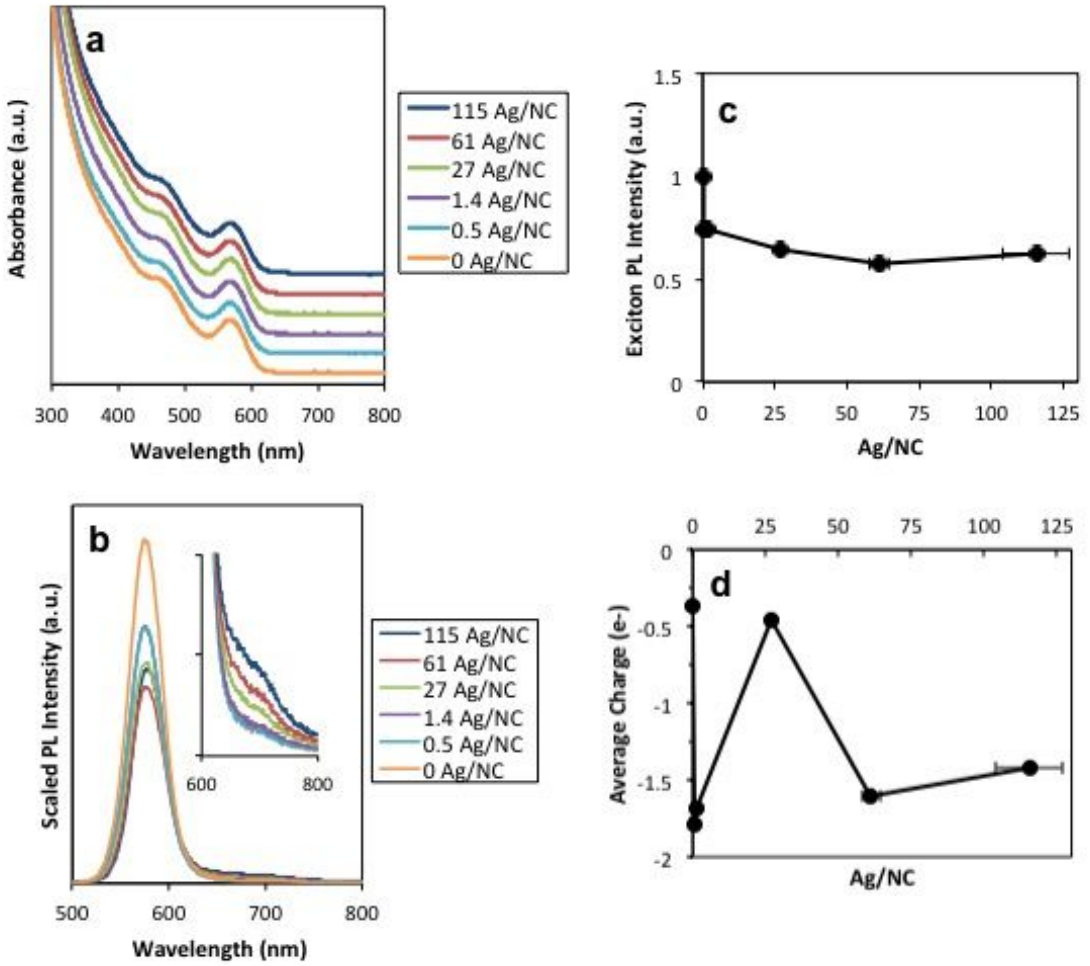

Figure S10. (a) Absorbance and (b) PL spectra for a set of Ag-CdSe NC doping. The inset in (b) magnifies the weak fluorescence feature near 700 nm. (c) The maximum exciton PL intensities and (d) the average charges vs. Ag/NC for this trial of Ag-CdSe.

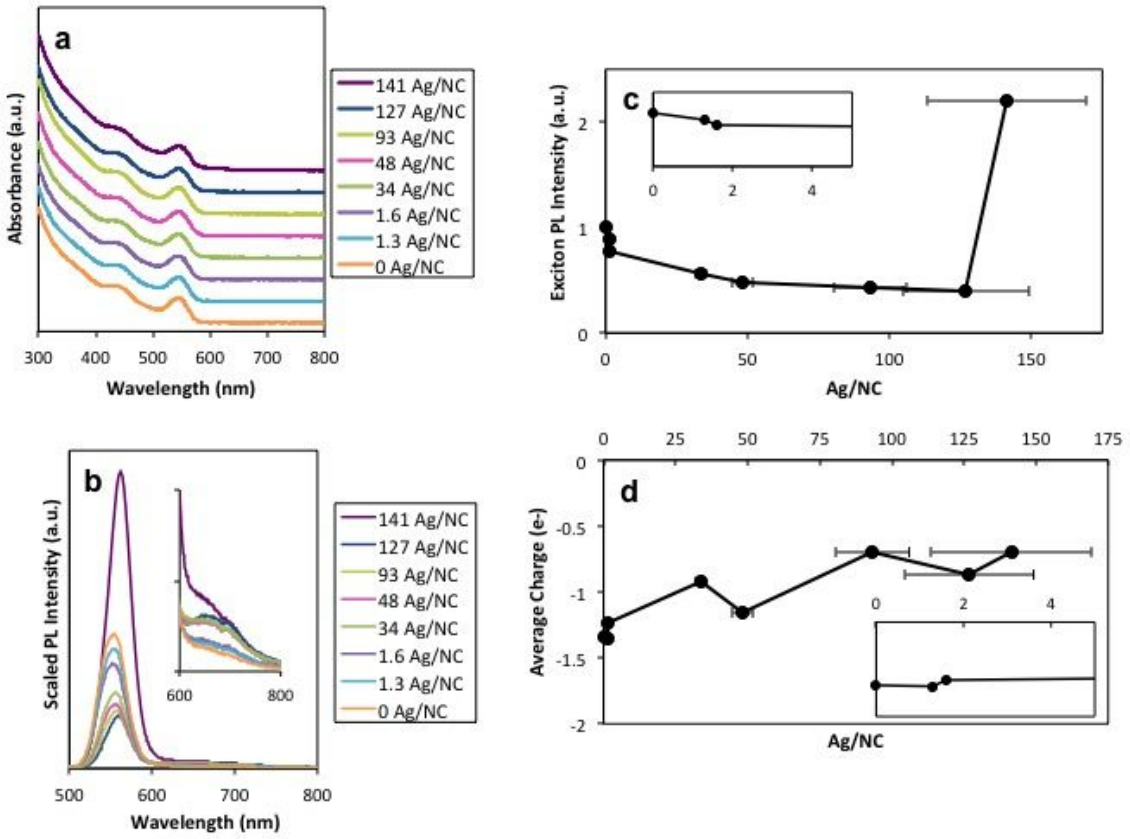

Figure S11. (a) Absorbance and (b) PL spectra for a set of Ag-CdSe NC doping. The inset in (b) magnifies the weak fluorescence feature near 700 nm. (c) The maximum exciton PL intensities and (d) the average charges vs. Ag/NC for this trial of Ag-CdSe.

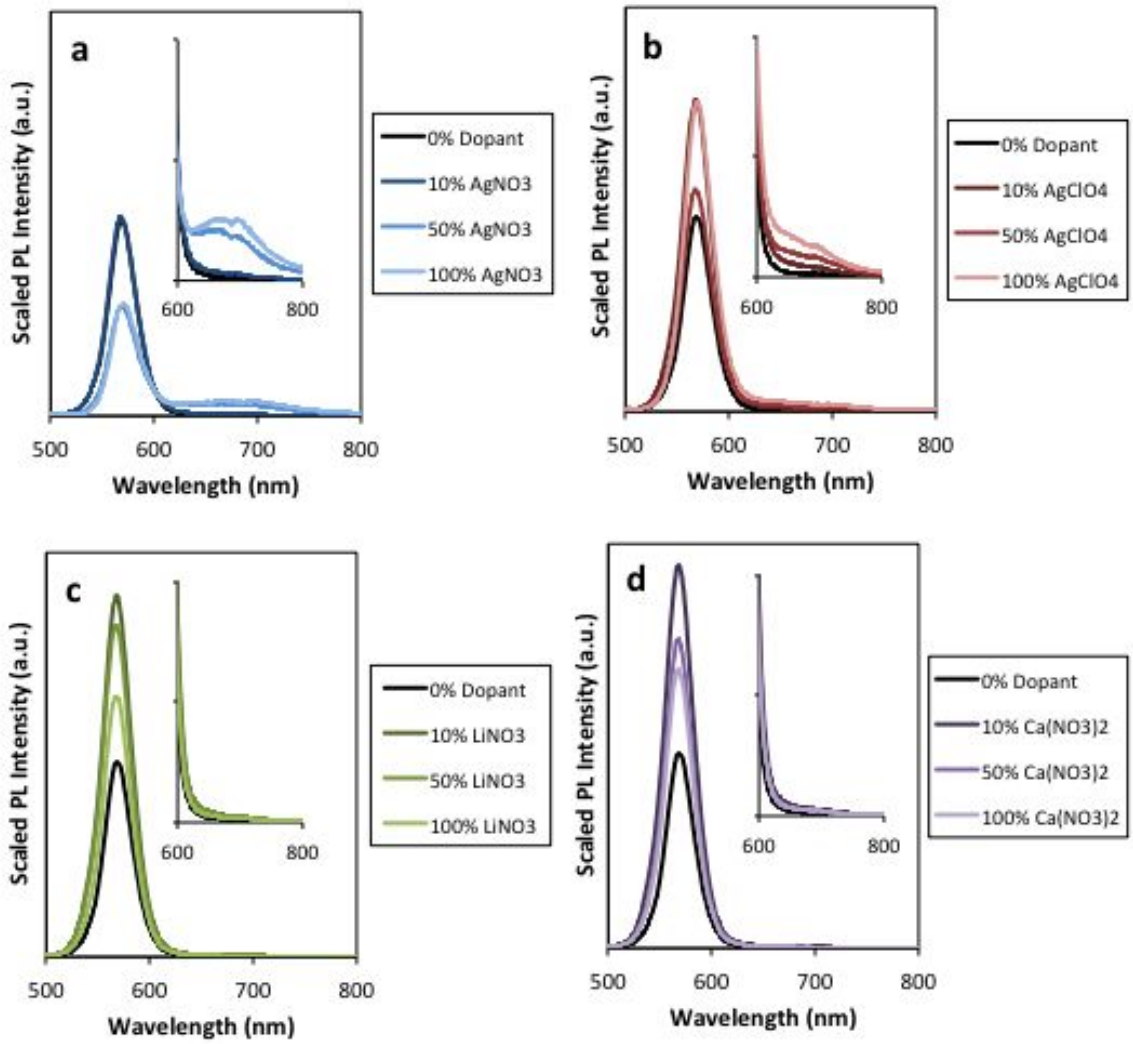

Figure S12. PL spectra for sets of CdSe doped with ethanolic solutions of (a) $AgNO_3$, (b) $AgClO_4$, (c) $LiNO_3$, and (d) $Ca(NO_3)_3$. The insets in these plots magnify the spectra near 700 nm showing a weak fluorescence feature in this range for the $AgNO_3$ and $AgClO_4$ trials.

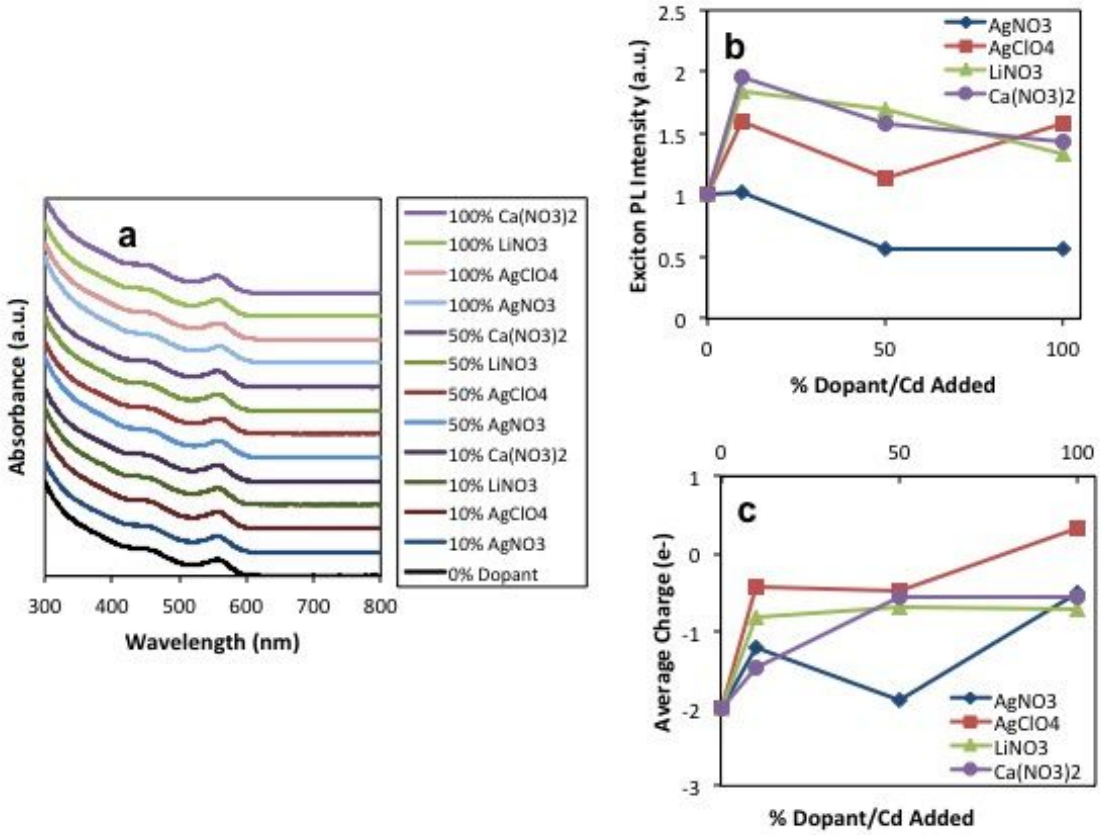

Figure S13. (a) Absorbance spectra for the same samples described in Figure S12. (c) The maximum exciton PL intensities and (d) the average charges vs. added dopant/Cd expressed as a percentage for these $AgNO_3$, $AgClO_4$, $LiNO_3$, and $Ca(NO_3)_2$ trials.

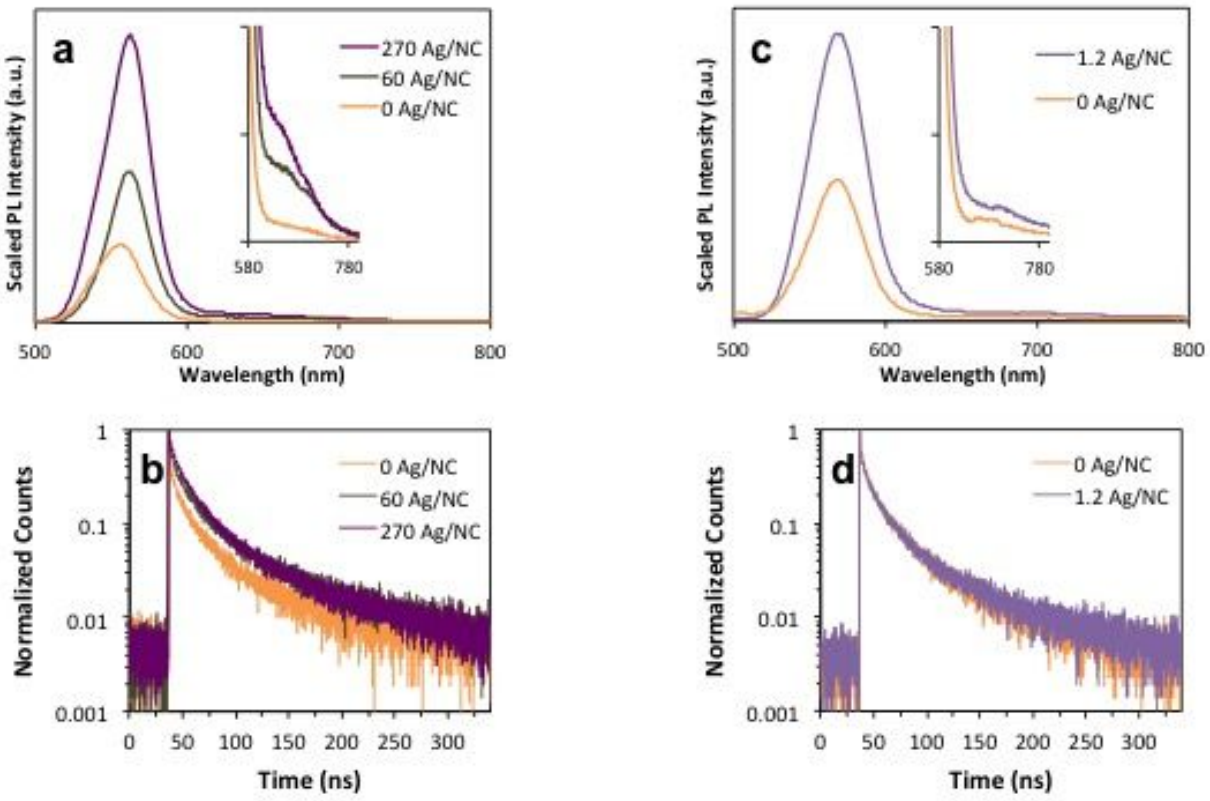

Figure S14. (a) Ensemble PL spectra for samples of Ag-CdSe NCs corresponding to the samples given in Figure 1 in the main paper. The inset in (a) magnifies the weak fluorescence feature near 700 nm. (b) The lifetime decay curves for the Ag-CdSe samples in (a). (c) Ensemble PL spectra for samples of Ag-CdSe NCs corresponding to the samples given in Figure S8. The inset in (c) magnifies the weak fluorescence feature near 700 nm. (d) The lifetime decay curves for the Ag-CdSe samples in (c).

Table S1. Measured lifetime data for Ag-CdSe samples calculated from the lifetime decay curves in Figure S14(b).

	A1 (%)	τ1 (ns)	A2 (%)	τ2 (ns)	Amplitude weighted lifetime (ns)	Average lifetime (ns)	Quantum yield (%)	Radiative rate (1/ns)	Nonradiative rate (1/ns)	% change k_{rad}	% change k_{nr}
0 Ag/NC	72.75	5.52	27.25	39.44	14.76	30.22	1.4	4.5×10^{-4}	3.3×10^{-2}		
60 Ag/NC	73.16	8.50	26.84	52.51	20.31	39.04	2.2	5.6×10^{-4}	2.5×10^{-2}	24	-23
270 Ag/NC	75.59	11.53	24.41	52.65	21.57	36.04	8.7	2.4×10^{-3}	2.5×10^{-2}	430	-22

Table S2. Measured lifetime data for Ag-CdSe samples calculated from the lifetime decay curves in Figure S14(d).

	A1 (%)	τ1 (ns)	A2 (%)	τ2 (ns)	Amplitude weighted lifetime (ns)	Average lifetime (ns)	Quantum yield (%)	Radiative rate (1/ns)	Nonradiative rate (1/ns)	% change k_{rad}	% change k_{nr}
0 Ag/NC	71.14	7.40	28.86	41.44	17.23	31.03	1.1	3.5×10^{-4}	3.2×10^{-2}		
1.2 Ag/NC	73.77	7.00	26.23	43.75	16.64	32.35	1.7	5.3×10^{-4}	3.0×10^{-2}	51	-5

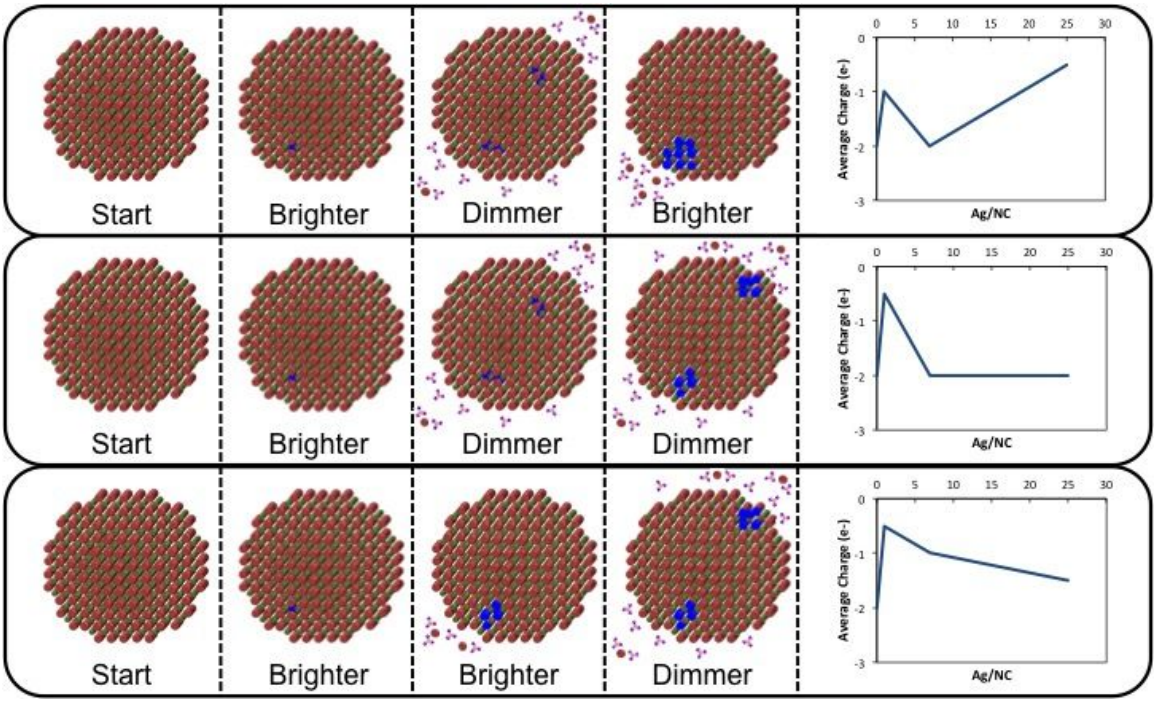

Figure S15. Cartoons that demonstrate different possibilities for introduction of dopants into NCs that help to explain the different trends in PL intensity/charge across doping trials and the correlation between PL intensity and charge.

4. References

1. Yu, W. W.; Peng, X. *Angew. Chem., Int. Ed.* **2002,** 41, 2368-2371.

2. Bullen, C. R.; Mulvaney, P. *Nano Lett.* **2004,** 4, 2303-2307.

3. Sahu, A.; Kang, M. S.; Kompch, A.; Notthoff, C.; Wills, A. W.; Deng, D.; Winterer, M.; Frisbie, C. D.; Norris, D. J. *Nano Lett.* **2012,** 12, 2587-2594.

4. Yu, W. W.; Qu, L.; Guo, W.; Peng, X. *Chem. Mater.* **2003,** 15, 2854-2860.

5. Shannon, R. D. *Acta Crystallogr.* **1976,** A32, 751-767.

6. Savitzky, B. H.; El Baggari, I.; Clement, C. B.; Waite, E.; Goodge, B. H.; Baek, D. J.; Sheckelton, J. P.; Pasco, C.; Nair, H.; Schreiber, N. J.; Hoffman, J.; Admasu, A. S.; Kim, J.; Cheong, S.-W.; Bhattacharya, A.; Schlom, D. G.; McQueen, T. M.; Hovden, R.; Kourkoutis, L. F. *Ultramicroscopy* **2018,** 191, 56-65.

7. Krauss, T. D.; Brus, L. E. *Phys. Rev. Lett.* **1999,** 83, 4840-4843.

8. Cherniavskaya, O.; Chen, L.; Weng, V.; Yuditsky, L.; Brus, L. E. *J. Phys. Chem. B* **2003,** 107, 1525-1531.

9. Krauss, T. D.; Brus, L. E. *Mater. Sci. Eng.* **2000,** B69-70, 289-294.

10. Krauss, T. D.; O'Brien, S.; Brus, L. E. *J. Phys. Chem. B* **2001,** 105, 1725-1733.

11. Cherniavskaya, O.; Chen, L.; Islam, M. A.; Brus, L. *Nano Lett.* **2003,** 3, 497-501.